# Modeling Of Metabolic Heat Regenerated Temperature Swing Adsorption (MTSA) Subassembly For Prototype Design

Chad E. Bower[1], Sebastian A. Padilla[2], and Christie S. Iacomini[3]
*Paragon Space Development Corporation, Tucson, AZ, 85714*

Heather L. Paul[4]
*NASA Johnson Space Center, Houston, TX, 77058*

This paper describes modeling methods for the three core components of a Metabolic heat regenerated Temperature Swing Adsorption (MTSA) subassembly: a sorbent bed, a sublimation (cooling) heat exchanger (SHX), and a condensing icing (warming) heat exchanger (CIHX). The primary function of the MTSA, removing carbon dioxide from a space suit Portable Life Support System (PLSS) ventilation loop, is performed via the sorbent bed. The CIHX is used to heat the sorbent bed for desorption and to remove moisture from the ventilation loop while the SHX is alternately employed to cool the sorbent bed via sublimation of a spray of water at low pressure to prepare the reconditioned bed for the next cycle.

This paper describes subsystem heat a mass transfer modeling methodologies relevant to the description of the MTSA subassembly in Thermal Desktop and SINDA/FLUINT. Several areas of particular modeling interest are discussed. In the sorbent bed, capture of the translating carbon dioxide ($CO_2$) front and associated local energy and mass balance in both adsorbing and desorbing modes is covered. The CIHX poses particular challenges for modeling in SINDA/FLUINT as accounting for solids states in fluid submodels are not a native capability. Methods for capturing phase change and latent heat of ice as well as the transport properties across a layer of low density accreted frost are developed. This extended modeling capacity is applicable to temperatures greater than 258 K. To extend applicability to the minimum device temperature of 235 K, a method for a mapped transformation of temperatures from below the limit temperatures to some value above is given along with descriptions for associated material property transformations and the resulting impacts to total heat and mass transfer. Similar considerations are given for the SHX along with functional relationships for areal sublimation rates as limited by flow mechanics in the outlet duct.

[1] Sr. Thermal Analyst, 3481 E. Michigan Street Tucson, AZ, 85714
[2] MTSA Project Lead, 3481 E. Michigan Street Tucson, AZ, 85714
[3] Acting Director of Operational Programs, 3481 E. Michigan Street Tucson, AZ, 85714
[4] Constellation Space Suit PLSS Ventilation Subsystem Lead, Space Suit and Crew Survival Systems Branch, Crew and Thermal Systems Division, 2101 NASA Parkway, Mail code EC5.

## Nomenclature

$a_e$ = evaporation coefficient
$A_{cross}$ = total cross sectional area of the sorbent bed
$c$ = sonic velocity
$C_1$ = system efficiency constant
$C_2$ = threshold loading fraction for proportional flow control
$C_3$ = desorption mass flow reduction factor
$C_4$ = desorption limit flow constant
$Cp$ = Specific heat at a constant pressure
$Cv$ = Specific heat at a constant volume
$dA$ = cross section of the unit volume
$D_h$ = hydraulic diameter
$D_{AB}$ = mass flow rate per unit area
$F$ = loading mass fraction
$\bar{f}$ = friction factor
$h_l$ = heat of desorption
$h_{vol}$ = volumetric heat transfer coefficient
$\Delta h$ = solid to vapor phase change energy
$\Delta h_{fg}$ = phase change energy from gas to liquid
$h_v$ = vapor heat transfer coefficient
$k$ = thermal conductivity
$k_f$ = frost thermal conductivity
$\dot{m}$ = mass flow rate
$\dot{m}''$ = mass flow rate per unit area
$m_{ice}$ = mass of ice
$M$ = Mach
$M_A$ = molecular mass of constituent A
$M_B$ = molecular mass of constituent B
$Nu$ = Nusselt number
$P$ = pressure
$\dot{q}$ = heat flow rate
$\dot{q}''$ = heat flow rate per unit area
$R_{gas}$ = individual gas constant
$Re$ = Reynolds number
$T$ = temperature
$t$ = time
$V$ = volume
$V_A$ = Diffusion volume of constituent A
$V_B$ = Diffusion volume of constituent B
$X$ = flow $CO_2$ mass fraction
$\gamma$ = ratio of specific heats
$\eta$ = efficiency
$\rho$ = density
$\rho_f$ = frost density

Subscripts:

$_{bed}$ = of the sorbent bed
$_{bulk}$ = bulk or free stream
$_{CO2}$ = Carbon Dioxide
$_{Ci}$ = concentration at interface
$_{C\infty}$ = concentration in free stream
$_{d}$ = based on hydraulic diameter

| | | |
|---|---|---|
| *dV* | = | discretized unit volume |
| *env* | = | SHX chamber environment |
| *flow* | = | of the bulk flow |
| *i* | = | at interface |
| *in* | = | into |
| *min* | = | minimum |
| *n* | = | new |
| *NCG* | = | non condensable gas |
| *o* | = | old |
| *s* | = | ice surface exposed to SHX chamber environment |
| *sat* | = | saturation |
| *tank* | = | in a unit volume $CO_2$ storage tank |
| *tot* | = | total |
| *wall* | = | at wall |

## I. MTSA System Overview

Metabolic heat regenerated temperature swing adsorption (MTSA) that is incorporated into a Portable Life Support System (PLSS) is being developed to remove and reject carbon dioxide ($CO_2$) from the space suit ventilation loop. Several studies have been performed to explore the concept [1-4]. A schematic of the proposed system is shown in Figure 1 and a brief explanation is provided here. Expired $CO_2$ in the ventilation loop is passed through and selectively collected by a molecular sieve consisting of 13X sorbent, also known as NaX zeolite. The ability of NaX sorbent to adsorb $CO_2$ increases with increasing pressure and decreases with increasing temperature. In the MTSA cycle, $CO_2$ loading occurs at a relatively low temperature and pressure, and is rejected by a combination of exposure to ambient pressure and increase in the bed temperature. This functionality is diagramed for Mars and Lunar operation in Figure 2. This temperature swing is achieved by alternating utilization of sublimating coolant (as low as 210 K to 250 K, depending on the fluid) and the energy that is present in the warm, moist ventilation loop exhaust (up to ~280 K). To provide continuous adsorption of $CO_2$, the technology relies on two separate beds that cycle between cold and warm modes, encouraging $CO_2$ adsorption and desorption, respectively.

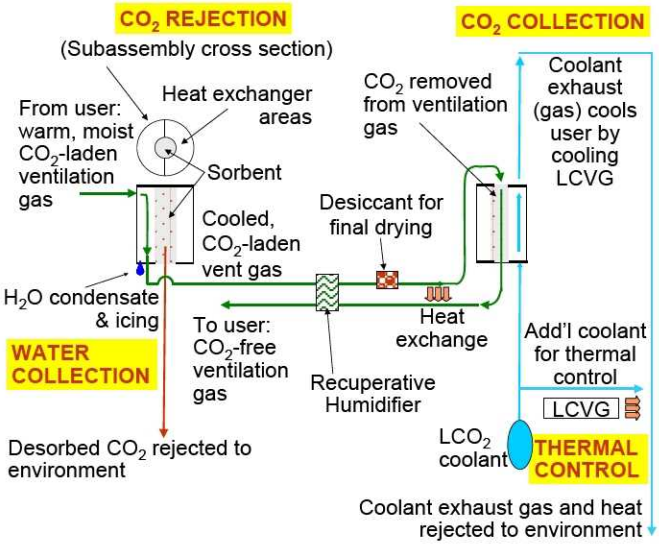


**Figure 1. Schematic Illustrating Two-bed MTSA Subsystem Operation**

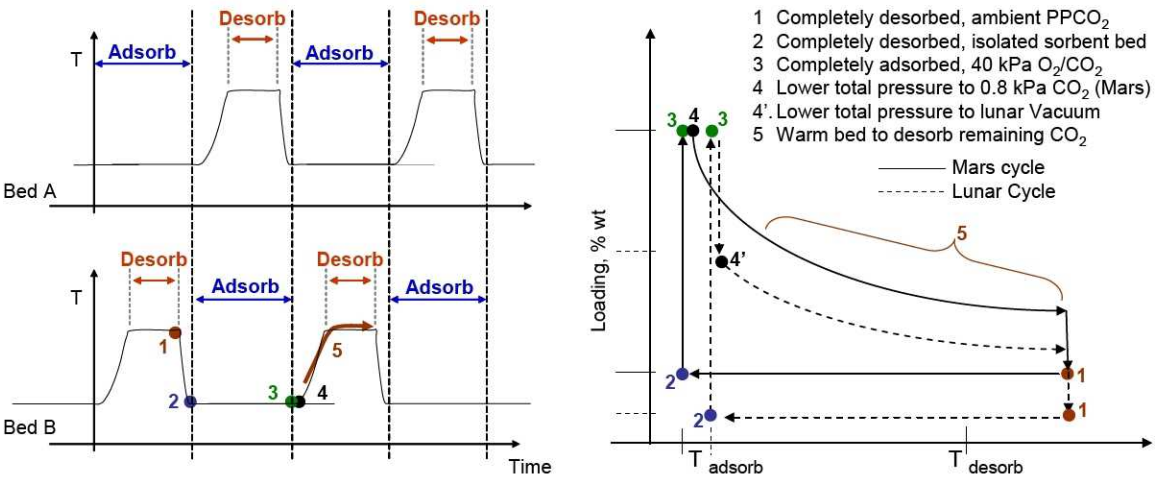


**Figure 2. Temperature (and Pressure) Swing Used to Regenerate the Sorbent Bed in Mars or Lunar Applications**

Each sorbent bed must be in contact with two separate heat exchangers: one for cooling (a sublimation heat exchanger that exhausts its coolant to the environment), and one for warming (condensing ice heat exchanger that uses the warm, exhausted ventilation loop flow before it is recycled in the PLSS). To minimize sorbent contamination, the bed must be isolated from both of the heat exchangers. These heat exchangers cannot be combined into one because of the vent loop volume that would be lost with each cycle when the sublimator coolant is exhausted to the environment. The heat exchangers must also be well connected to the system to allow for efficient energy exchange. A view of the primary MTSA subassembly containing the sorbent bed, condensing ice heat exchanger (CIHX) and sublimation heat exchanger (SHX) is shown in Figure 3. The following sections describe the operation and modeling methods used in the development of a MTSA subassembly model that will be used to support design of a unit suitable for use in a space suit ventilation loop while operating in a lunar environment.

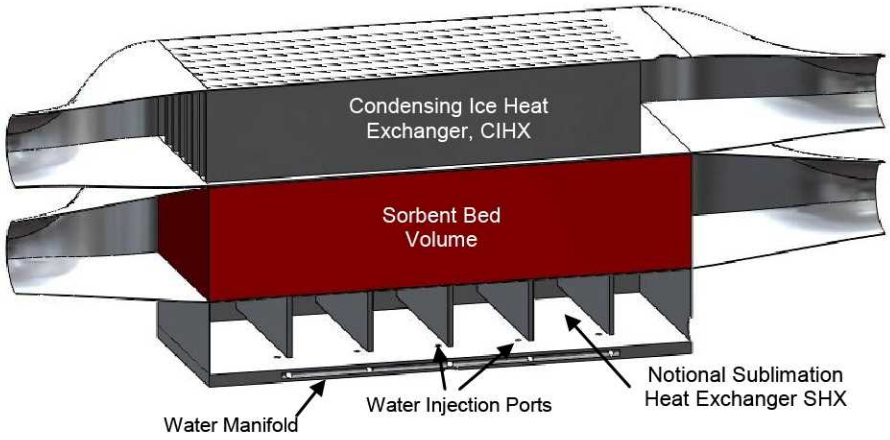


**Figure 3. MTSA subassembly cut view showing the three primary subsystems**

### A. Sorbent Bed Overview

The $CO_2$ adsorption phase of the MTSA cycle handles a constant flow of a process gas, a mixture primarily consisting of $O_2$ and $CO_2$ with small amounts of water vapor and other trace contaminants which can be neglected. This flow passes through the porous adsorbent bed consisting of an open cell aluminum foam, wash coated with sorbent NaX. The flow transfers heat to the solid media, quickly equilibrating with the bed temperature, as well as transferring $CO_2$ mass. As the material nearest the inlet approaches holding capacity, $CO_2$ laden gas will travel over the filled portions of the bed until reaching unsaturated sorbent. This sets up a $CO_2$ front and the associated exothermic process at this front drives a thermal gradient through the bed. Since the amount of $CO_2$ that the bed can adsorb is inversely proportional to temperature, any energy deposited from the process flow and exothermic reactions is adverse to the capacity of the bed and needs to be removed by a heat exchange process. The local mechanism for moving this heat from the sorbent bed to the walls for removal by the SHX is the porous aluminum foam. Development of a discretized sorbent bed model allows for evaluation of design dimensions (length, width, and thickness) and allows for assessment of the effectiveness of solid fins if necessary. The developed adsorption modeling methodology is also implemented to model the desorption portion of the cycle where the bed is exposed to lunar vacuum and heated via the CIHX to drive off the adsorbed $CO_2$.

### B. Sublimation Heat Exchanger overview

As shown in Figure 2, the loading capacity of the sorbent bed increases as the sorbent temperature decreases. Since adsorption is exothermic and the process flow is supplied at ~280 K, the bed must be actively cooled while it is removing $CO_2$ from the ventilation loop. For Mars application, the baseline method for cooling the bed is to expand liquid $CO_2$ stored at ~6000 kPa (~900 psi) to ambient pressure (~0.8 kPa) through a valve, whereupon it cools to ~150 K. This cool gas / solid mixture then travels through a tube attached to the sorbent bed that serves to operate as a SHX. $CO_2$ was chosen for the coolant due to in-situ resource availability. For Lunar application, an analogous solution is proposed where liquid water is used as the coolant source since $CO_2$ is not available in the environment and water is a more mass efficient coolant. Expansion of water to temperatures comparable to a $CO_2$ system however, requires reduction of operating pressure by more than 4 orders of magnitude. Restrictive passages such as tubes will not allow sufficient mass flow at the pressures required to cool the system via sublimation. Instead the proposed system sprays expanded water in a solid/gas mixture near ~235 K onto a surface to be cooled. The solid subsequently sublimates carrying away system heat. A simplified version of a SHX in a lunar configuration is shown in Figure 4. The reference mass that requires heat extraction, in this case the sorbent bed, is represented in red (on the left). The blue surface represents the sublimation surface where the coolant water is sprayed. Sublimation drives water vapor into the chamber, shown in gray, and the vapor travels down an exhaust duct (to the right) where it exits to a lower pressure environment.

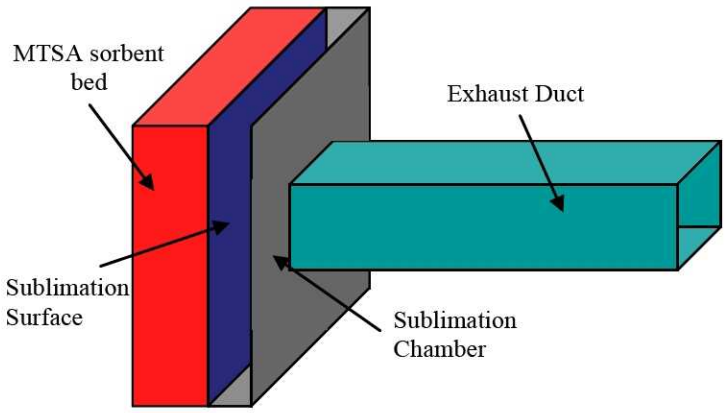


**Figure 4. General SHX Component Modeling Description**

### C. Condensing Ice Heat Exchanger overview

The CIHX is employed to extract metabolic heat from a process flow in order to warm the sorbent bed. This temperature swing supports $CO_2$ desorption as shown in Figure 2. In the currently considered lunar case, exposure of the sorbent bed to lower $CO_2$ partial pressures, specifically lunar vacuum, also encourages desorption by reducing the NaX loading capacity. In the CIHX, warm, humid gas exchanges heat with walls initially cooled to around 235 K by the SHX, with a goal of heating the sorbent bed to 280 K. As the $O_2$/ water vapor mixture flowing through the exchanger is cooled below the dew point, condensation forms on the heat exchange surfaces. While the surfaces remain below 273 K, the condensate forms as a low density frost on the surfaces [7]. As the bed warms to near

273 K, ice formation stops and the layer of deposited ice begins to melt while water ice continues to be deposited in a liquid form. Surface tension draws the liquid water into the ice layer, at first densifying the layer since the underlying surface remains below freezing, then melting it. When the interstitial spaces between the remaining ice is full, water begins to run off the bed and can be collected. Eventually, all the ice melts and liquid condensation occurs directly on the heat exchanger surfaces for surface temperatures below the dew point.

## II. System Modeling

Heat and mass transfer can be treated at the system level as a "black box" where heat and mass are transferred based on an understanding of the system efficiency. While this type of model works well for doing system trades for first order design [10], a higher fidelity system model that captures the details of local heat and mass transfer is required in order to validate the larger systemic parametric efforts, to refine assessments of system performance, and support design revision and optimization. To this end, a modeling methodology was developed for each of the described subsystems. This paper primarily speaks to development of the relevant heat and mass transport and energy storage characteristics of each subsystem with the intent that they can be coupled with the solid conduction analysis capabilities of a general purpose thermal analyzer. The specific set of thermal software chosen for implementation of this modeling methodology is C&R Technologies Thermal Desktop® 5.x2 patch 5 with SINDA/FLUINT patch level 7. This allows for development of a detailed, discretized thermal model of the MTSA subsystem and localized descriptions of the physical processes that occur within the subassembly.

### A. Sorbent Bed

#### 1. *Sorbent Bed Discretization*

The methods developed for modeling mass and heat transfer through the sorbent bed are based on the flow and thermal characteristics of a flow through a porous media. Modeling of flow through a porous media is significantly different from free internal flow. In free internal flow, resistances are exerted only from the walls of the enclosure resulting in a hydrodynamically developing flow gradient along the duct; however, in a porous media, the distributed surface area and associated resistance results in a near constant velocity profile through the bed. This flow property allows for discretization of the flow to be paired with thermal discretization of the sorbent bed media. A conceptual view of such a discretized flow as developed in Thermal Desktop for a rectangular sorbent bed is shown in Figure 5.

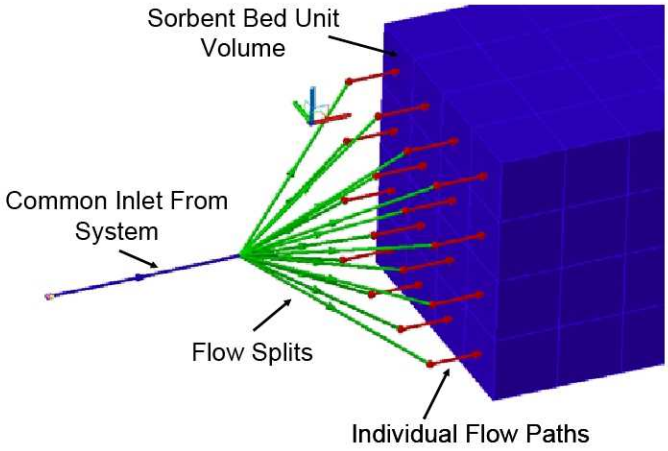


**Figure 5. Sorbent bed volume and flow discretization.**

The blue path labeled "common inlet from system" contains the total input mass flow rate. This flow splits into smaller parallel flows in the red paths and continues through the discretized volumes, dV, shown in blue. Figure 6 shows a detailed view of a representative discretized volume. As in Figure 5, the primary flow through the volume is represented in red and contains the resistance to bulk flow through the volume. The primary flow path is thermally connected via the green Thermal Desktop tie to the unit volume solid thermal mass, which is shown in blue. $CO_2$ mass transfer is handled

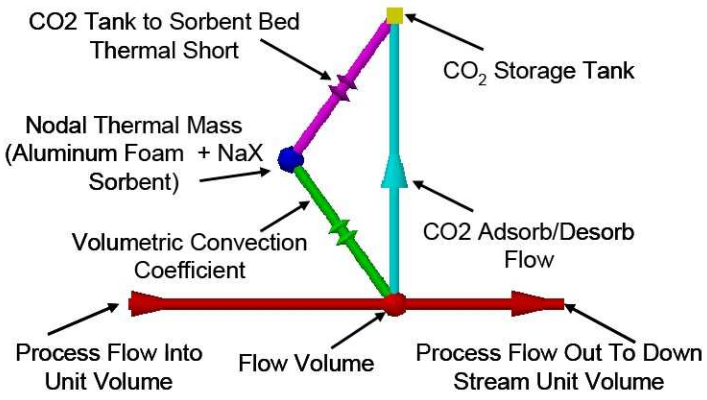


**Figure 6. Flow and heat transfer specifics at each discretized unit.**

in the light blue path which connects the primary process flow to a storage tank which represents a $CO_2$ mass storage potential of the unit volume. Since adsorbed $CO_2$ mass is held in intimate contact with the sorbent bed, the storage tank is thermally shorted to the nodal mass by a tie with a large conductance.

*2. Sorbent Bed Material Properties*

The primary parameters of interest in the sorbent bed are the thermal conductivity and the specific heat of the bed materials. The Duocel® open cell aluminum substrate to which the NaX washcoat is applied is a 40 pores per inch foam with 8% density manufactured by ERG aerospace. The composite density of this bed is the sum of the foam mass per unit volume which is 216.5 kg/m$^3$ at 8% density plus the calculated effective density of the NaX sorbent. The effective density of the sorbent can be determined as the difference in mass before and after wash coating divided by the volume of the sorbent bed. From testing [5], the effective sorbent density has been calculated to be 77 kg/m$^3$ on average, resulting in a total effective density of 293.5 kg/m$^3$. Since NaX washcoat is a small fraction of the total bed mass, about 25%, and its specific heat can be presumed on the order of aluminum, the published value of 896 J/kg-K for Al 6061 can be used with an expected error of less than 10%. The thermal conductivity of this foam is approximately 10.0 W/m-K as reported by the manufacturer [9]. While the thermal conductivity of the NaX washcoat is unknown, it is a ceramic like material and can be expected to have thermal conductivity of 1-2 orders of magnitude lower than Aluminum. This paired with the low mass fraction of washcoat allows direct use of the foam thermal conductivity for the composite bed thermal conductivity.

Since the flow is being modeled directly and the rates are known, the latent heat of desorption for $CO_2$ can be applied to the fluid storage tank (or nodal mass for model stability) by multiplying the flow rate times the adsorption/ desorption energy to give an accurate input heat rate for the control volume.

*3. Adsorption Mass Transfer and Associated Control Logic*

Per the assumptions of a porous media, the flow into the bed is presumed to be equally distributed at the inlet. This would indeed mimic the design intent to efficiently use the sorbent in the bed. Thermal gradients in the bed will occur, especially as the current baseline assumes the bed is cooled by the SHX on one side only. Since the loading capacity of the sorbent is dependant on temperature there is the possibility for small amounts of cross flow; however, since the mass fraction of $CO_2$ in the process flow is small, the effect of these cross flows is considered negligible and the flows can be tracked independently. Thus at the inlet the flow into a unit volume is:

$$\dot{m}_{dV\,in} = \dot{m}_{tot} \frac{dA_{cross,dV}}{A_{cross,tot}} \tag{1}$$

Where $A_{cross,\,tot}$ is the total cross sectional area and dA is the cross section of the unit volume. Since all of the unit volumes can be divided into equal cross section areas (and length) the mass flow in to each unit volume at the inlet is equal. This mass flow rate passes through each of the subsequent paths minus the portion of $CO_2$ removed.

In previous studies with this sorbent, downstream measurements indicate that the process flow exits the bed fully depleted of $CO_2$ until breakthrough occurs at which point the outlet $CO_2$ mass fraction approaches the inlet value. From this we assume that the flow reaches quasi-equilibrium with the bed over small distances relative to the bed dimensions. This assumption enables a key assumption in the modeling. The developed adsorption logic is designed to achieve and maintain levels of bed loading during the adsorption cycle. This is to say that the bed seeks equilibrium with the local flow without considering a diffusion rate limit. The first step in any of the logic paths is to determine the loading for a given unit volume. This loading capacity of the sorbent bed is qualified in terms of the mass of loaded $CO_2$ to the mass of the dry, unladened sorbent as functions of pressure and temperature (which can be determined empirically for our assumed design [5]). With equal sized discretized volumes the sorbent mass is divided equally among *n* discretized volumes. The unit volume sorbent mass is paired with a tabular form of the sorbent performance data to give the saturated capacity of the control volume, $m_{sat}$. This value is compared to the current amount of $CO_2$ mass stored in the volume, $m_{tank}$, to determine the loading fraction by the equation:

$$F = \frac{m_{tank}}{m_{sat}} \tag{2}$$

For loading fractions, F, below a dead band value (nominally 99% of the holding capacity), the local sorbent is considered unsaturated and available to adsorb of $CO_2$ if it is available in the local process stream. This is accomplished by determining if the ratio of the $CO_2$ mass fraction in the flow entering the unit volume to the value entering the system is greater than a threshold value:

$$\frac{X_{sys\ in}}{X_{dV\ in}} \geq C_1 \tag{3}$$

Where $X_{dV\ in}$ is the $CO_2$ mass fraction entering the unit volume, $X_{sys\ in}$ is the system inlet $CO_2$ mass fraction and $C_1$ the threshold constant, nominally 1%. Since $CO_2$ is removed form the process flow until at least this threshold is attained, the minimum system efficiency, $\eta_{min}$, can be defined as:

$$\eta_{\min} = (1 - C_1) \tag{4}$$

Efficiency lower than 1.0 ensures that the code will not work to remove every small portion of $CO_2$ which can result in time step problems in SINDA/FLUINT. Similarly, the inlet mass flow rate is checked to ensure non zero system mass flow rates. If sufficient $CO_2$ exists in the incoming flow, the $CO_2$ extraction rate, $\dot{m}_{CO_2}$ is determined by:

$$\dot{m}_{CO_2} = X_{dV\,in}\dot{m}_{dV\,in} \tag{5}$$

For a combination of large time steps, small adsorbent volumes, and large $CO_2$ flow rates, the storage capacity of a unit volume to rise to a value above the dead band resulting in overshoot would require desorption in the subsequent time step. In order to avoid this, proportional control as a function of loading fraction is applied to the flow rate when the loading fraction is greater than $C_2$, nominally 80%, by the equation:

$$\dot{m}_{CO_2} = \dot{m}_{CO_2}\left[1 - \frac{F - C_2}{1 - C_2}\right] \tag{6}$$

This equation linearly reduces the flow rate into the control volume from 100% of available $CO_2$ flow at a loading fraction of $C_2$ to no flow at a loading fraction of 1.0, resulting in an asymptotic filling of the storage tank.

### 4. *Desorption Mass Transfer and Associated Control Logic*

For loading fractions greater than the deadband value, nominally 101%, flow is removed from the storage tank. Due to a large change in equilibrium loading potential when the bed is suddenly exposed to vacuum, the quasi equilibrium assumption made for adsorption is not valid in a desorption model. $CO_2$ desorption rates are restricted by diffusion limits and reaction kinetics. For system design these specifics are unnecessary to model, instead empirical rate limits can be derived to allow a response that matches previously gathered desorption data. Within this framework, mass flow calculation is first limited to a maximum flow rate that prevents abnormal termination of the simulation. This value is then refined to reflect expected system desorption characteristics. The maximum flow rate is calculated such that all of the excess mass contained at the beginning of a time step is removed by the end of the time step by:

$$\dot{m}_{CO_2} = \frac{C_3\left(m_{sat} - m_{tank}\right)}{t_n - t_o} \tag{7}$$

In this equation $t_n$ is the time at the current timestep and $t_o$ previous time step. The value of $C_3$ is nominally 0.5 or less for two reasons. First, a tank can not have a negative volume as values of 1.0 or greater could cause for a fixed time step. Second, time steps are not fixed so using the previous time step for calculation has some caveats. If the next time step is smaller than the previous, less mass will be removed than expected. This is of little consequence since the value is recalculated for the next time step. If the time step is larger however, the calculated flow would more than empty the tank. Fortunately, a time step in SINDA/FLUINT is restricted to a 2x growth between time steps, making a multiplier of 0.5 appropriate.

Large flow rates from the storage tanks would occur under this methodology during the sudden exposure to vacuum. This flow rate could in turn increase the bed pressure such that the next iteration would require adsorption causing instability in the model. To avoid this, a limiting equation is developed in lieu of a diffusion limit by:

$$\dot{m}_{CO_2} = \frac{C_4}{n} \tag{8}$$

Where n is the number of control volumes in the model and:

$$C_4 = -\left(\frac{\text{nominal inlet flow rate} * \text{desorb cycle time} * C_3}{\text{minimum desired desorption time}}\right) \tag{9}$$

The parameters in this or a similar equation will be derived as needed to yield expected desorption performance.

*5. Heat Transfer in the Sorbent Bed*

There are two sources for heat transfer in the sorbent bed model, convection from the warm process flow to the bed and adsorption/ desorption energy. Sorption energy is applied to the mass containing node of the control volume by the equation:

$$\dot{q}_{dV} = \dot{m}_{CO_2} h_l \tag{10}$$

Where $\dot{q}_{dV}$ is the applied heat rate to the unit volume and $h_l$ is the latent heat of desorption. Convection in the volume is handled via a volumetric heat transfer coefficient $h_{vol}$ ($W/m^3$-K).

$$\dot{q}_{dV} = h_{vol}\, dV (T_{flow} - T_{bed}) \tag{11}$$

Where $T_{flow}$ is the local flow temperature and $T_{bed}$ is the local bed temperature. The volumetric heat transfer coefficient can be determined from a correlation derived from experimental data for Doucel® foams of similar hydraulic diameters by the equation [11]:

$$Nu_d = b_1 \mathrm{Re}_d^{b_2} \tag{12}$$

In this equation, $b_1$ is 0.325 and $b_2$ is 0.601 for 5% dense foam, which is considered sufficiently close to the 8% dense foam used in this design. In addition to heat loads in the sorbent bed media, there are loads imposed on the bed by the sublimation and condensing ice heat exchangers that are described in the following sections.

## B. Sublimation Heat Exchanger

### 1. *Sublimation Mass Transfer*

The role of the SHX is to remove energy from the MTSA system. In this process, energy is moved across the sorbent bed to a cooled surface, the energy is removed from the surface by sublimation from a layer of ice, and a flow of evolved gas exits the system through an exhaust duct to lunar vacuum. The active component of the SHX consists of a surface of area, $A_s$, on to which water is sprayed. Feed water is supplied to one or more nozzles at a temperature of ~280 K and a pressure of 1 atm (101 kPa) where it undergoes an isenthalpic expansion to the chamber pressure. For pressures that bring the temperature below the triple point, the liquid water transforms into a solid/ vapor mixture with a quality near 0.15. The solid fraction, 0.85, can be considered to be evenly distributed over the SHX surface, while the remaining vapor is presumed to take no further part in energy exchange and is incorporated into the exit duct flow. When the deposited layer of ice is thin (as is an objective of the design), the temperature of the ice surface, $T_s$, exposed to the sublimation chamber can be considered equal to that of the heat exchanger surface. For a given ice surface temperature, the equilibrium ice surface pressure, $P_s$, can be determined by a formula attributed to Wexler [12]:

$$\ln(P_s) = \sum_{i=0}^{4} k_i T^{i-1} + k_5 \ln T_s \tag{13}$$

Where $k_0 = -5.86\text{x}10^3$,$k_1 = 2.23\text{x}101$, $k_2 = 1.39\text{x}10^{-2}$, $k_3 = -3.42\text{x}10^{-5}$, k4 = $2.70\text{x}10^{-8}$ and $k_5 = 6.70\text{x}10^{-1}$

Similar to the mechanism by which a temperature difference serves as the driving potential for heat transfer from a surface to a fluid, a mass transfer process is governed by a pressure difference. When the pressure in the sublimation chamber is lower than the ice surface pressure, water vapor sublimates from the ice surface in an isothermal expansion while the associated phase change results in energy transfer from the ice surface at a rate defined by the equation:

$$\dot{q} = \dot{m}\Delta h \tag{14}$$

Where $\dot{q}$ is the heat load rejected from the system, $\dot{m}$ is the surface mass flow and Δh is the phase change enthalpy for ice, which is approximately 2840 kJ/kg at 235 K. This mass flow rate can be expressed as [13]:

$$\dot{m} = \frac{A_s a_e (P_s - P_{env})}{\sqrt{2\pi R_{gas} T_s}} \tag{15}$$

Where $P_s$ is the ice surface equilibrium pressure at the ice surface temperature $T_s$, $P_{env}$ is the environment pressure, $R_{gas}$ is the individual gas constant for water, and $a_e$ is the evaporation coefficient. The evaporation coefficient can have a value between 0 and 1 and essentially accounts for inefficiency in the mass transfer process thought to occur due to collisions between sublimating molecules and molecules in the environment. For a high vacuum environment at 214 K, the value was shown to be approximately 0.07 with values increasing to 0.11 at higher temperatures. For the purposes of this modeling, 0.07 is used. Equation 15 can be used to express the chamber pressure, $P_{env}$, required to reject a given $\dot{m}$ at a given $T_s$. In addition, the phase change process and the pressure drop across the SHX chamber that carries the flow to the environment are both isothermal processes such that the gas temperature in the SHX chamber equals $T_s$. These values serve as inlet conditions to the resulting exit duct flow.

### 2. *Vent Duct Flow*

The exit duct forms the final link in removing energy from the sorbent bed. This process, like the mass transfer that precedes it, requires a pressure drop to move the gas from the duct inlet to the duct exit. The expansion of an ideal gas through a constant area duct to a vacuum can be characterized as frictional adiabatic flow. This process is neither isentropic nor isenthalpic; it is instead characterized as a fanno-line flow. In this type of flow the conditions

at the exit (temperature, pressure, and density) are dependant on the inlet conditions, the amount of friction force exerted on the flow by the duct along the path, the duct length and its hydraulic diameter. An analysis of this type begins with one important parameter assigned. Since the flow is vented to a vacuum, the flow accelerates to the sonic velocity at the exit of the duct. This can also be described as having an exit Mach number, M, of unity. The Mach number is defined as local velocity, V, divided by the local sonic velocity, c, [14]. Assuming the flow in the duct is an ideal gas, the sonic velocity is defined by:

$$c = \sqrt{TR_{gas}\gamma} \tag{16}$$

Where T is the local temperature, and $\gamma$ is the ratio of specific heats, $C_p/C_v$, which has a value of 1.3 for water. The local velocity is determined by the continuity equation:

$$\mathrm{V} = \frac{\dot{m}}{A_d \rho} \tag{17}$$

Where $A_d$ is the duct cross sectional area and $\rho$ is the local flow density as determined by the ideal gas law. For flow of this type, the Mach number at the inlet of the duct can be related to the length of the duct, $L_{max}$, the hydraulic diameter, $D_h$, and the average friction factor, $\bar{f}$ by:

$$\frac{L_{\max}\bar{f}}{D_h} = \frac{1-M^2}{M^2\gamma} + \frac{\gamma+1}{2\gamma}\ln\left[\frac{(\gamma+1)M^2}{2\left(1+\frac{\gamma-1}{2}\right)M^2}\right] \tag{18}$$

In this equation the Mach number based on the inlet conditions. Furthermore, since the Reynolds number is expected to be on the order of 100 or less, the flow is laminar and the friction factor is 64/Re. In practice the value of the friction factor is approximated for the duct inlet properties.

### 3. *Mass Flow Regimes*

For a given duct hydraulic diameter, combination of Eqns. 16 through 18 yields an expression that relates the required duct inlet parameters, $T_{in}$ and $P_{in}$ that satisfy the outlet condition of sonic flow for a given duct geometry and value of $\dot{m}$. These parameters are explicitly expressed by the heat and mass transfer derivation. When $\dot{m}$ is such that conditions of $T_{env}$ and $P_{env}$ are equivalent to $T_{in}$ and $P_{in}$, the capacity of the system to reject mass flow is equal to the amount of flow generated. In this state, the system can be described as operating at the critical mass flow rate.

In application, the provided mass flow may be lower than this critical mass flow rate, called a sub-critical mass flow rate. In this case, the supplied solid coolant mass still sublimates, but Eq. 14 dictates that the removed heat rate scales with the sublimation rate. For a fixed sorbent bed resistance, a reduced heat transfer rate results in a higher value for the SHX surface temperature, and thus Ts (assuming, again, the ice layer is thin). An increased $T_s$ in turn results in a greater $P_s$ and from Eq. 15 the process can take place at a higher environment pressure. On the duct side, reduced mass flow reduces the value of $P_{in}$ needed to move the flow through the duct. Thus, at subcritical mass flow rates, a state change occurs where $P_{env}$ reduces to $P_{in}$ through an isenthalpic expansion. Due to the small change in internal energy at these low pressures this expansion is approximately an isothermal one. In short, the rejected water vapor (both sublimated and the original ~ 15% by mass supplied in the coolant feed) undergoes an uncontrolled expansion in the sublimation chamber which aligns the inlet conditions with those required to reject the flow from the duct.

Conversely, for supercritical mass flow rates through the duct, the required duct inlet pressure, $P_{in}$, would be higher than the value of $P_{env}$ required to drive all of the deposited mass flow from the SHX surface. In this case $P_{env}$ again equals $P_{in}$ and mass flow is limited to the critical mass flow rate, with one difference. While part of the additional mass flow can be deposited as an ice layer on the sublimation surface, the additional gas evolved during the isenthalpic expansion in the nozzle must still exit the system. This results in a reduced allowance for sublimation mass which results in operation below the critical mass and heat rejection rates. This effect is initially minimal for flow rates less than a few times the critical flow rate due to the 0.15 quality that enters the sublimation chamber, but over time can be compounded by reduced surface temperature if the accumulated ice layer becomes thick enough to achieve significant thermal resistance. From a system view, inlet (nozzle) mass flow rates above the critical mass flow rate result in no change in outlet mass flow (from the duct) and result in reduced heat rejection from the system.

### C. Condensing Ice Heat Exchanger

#### *1. Heat and Mass Transfer Modeling Methodology*

The primary modeling challenge in the CIHX is the simulation of both the effects of heat and mass transfer to and through the heat exchanger surface. To this end, heat and mass transfer relationships could be developed and directly implemented in any programming language. However SINDA/FLUINT, the solution engine for Thermal Desktop, contains routines for handling both heat and condensation mass transfer suitable to this task. The applicable SINDA/FLUINT formulation is detailed in this section.

Convection heat transfer form the vapor flow is handled by the general heat transfer equation:

$$\dot{q}'' = h_v(T_{bulk} - T_i) \tag{19}$$

Where $h_v$ is the vapor heat transfer coefficient, $T_{bulk}$ is the local mixed mean fluid temperature and $T_i$ is the local interface temperature. The heat transfer coefficient is developed from standard Nusselt number correlations for laminar, transitional, or turbulent flow based on Reynolds number. Flows in the CIHX are expected to be in the laminar regime [6].

Mass transfer in SINDA/FLUINT is handled in a generally applicable heat to mass transfer parallel known as the Chilton-Coulburn analogy. In this formulation, the local mass flux on a surface in contact with a fluid carrying a condensable species is described as a function of total and constituent states including density, $\rho$, and pressure P, as well as fluid properties including mass diffusivity, $D_{AB}$, thermal conductivity, and specific heat by the equation [17]:

$$\dot{m}'' = h_v * (\rho_{C\infty} - \rho_{Ci}) * \left[ \frac{P_{Tot}}{P_{NCG}} * \rho_{NCG\infty} * \frac{\ln\left(\frac{\rho_{NCGi}}{\rho_{NCG\infty}}\right)}{\rho_{NCGi} - \rho_{NCG\infty}} \right] * \left[ \rho * C_p * \left( \frac{k}{D_{AB}} \right)^2 \right]^{-\frac{2}{3}} \tag{20}$$

In this formulation, the subscript $_{C\infty}$ denotes concentration in the free stream; $_{Ci}$ is the concentration at the interface, $_{tot}$ is total rather than partial pressure, and $_{NCG}$ refers to a non condensable gas. Properties are evaluated at free stream conditions unless otherwise noted. In this equation all of the terms on the right hand side other than $(\rho_{C\infty} - \rho_{Ci})$ can be combined to form a term analogous to a heat transfer coefficient, while $(\rho_{C\infty} - \rho_{Ci})$ is the gradient which drives the mass transfer. In Eqn. 24, the mass diffusivity is estimated by [17]:

$$D_{AB} = \frac{10^{-3} T^{1.75} [M_A + M_B / (M_A M_B)}{P_{tot} \left[ \left( \sum V \right)_A^{1/3} + \left( \sum V \right)_B^{1/3} \right]^2} \tag{21}$$

Where $M_A$ and $M_B$ are the molecular masses of the non condensable gas and water constituents, and $\Sigma V_A$ and $\Sigma V_B$ are the diffusion volumes. Since heat transfer and mass transfer effects superpose, the mass transfer equation can be thought to operate in parallel with the heat transfer equation. The phase change energy associated with the condensation that accompanies this mass flow can be described by:

$$\dot{q}'' = \dot{m}'' \Delta h_{fg} \tag{22}$$

Where $h_{fg}$ is the enthalpy difference between the gas and fluid phases. Note that the heat and mass transfer equations are evaluated at interface conditions. When a condensate is present, this interface is the liquid to vapor interface, allowing for the effect of an additional film resistance that occurs at the surface. Heat flow through this resistance can be termed as:

$$\dot{q}'' = h_{film} (T_i - T_{wall}) \tag{23}$$

Where Twall is the actual solid surface temperature and $h_{film}$ is the condensation heat transfer coefficient based on Rohsenow's correlation. In practice this resistance is automatically calculated and applied by the SINDA/FLUINT command ROHSEN [17]. While a condensate is present, the resulting series/ parallel arrangement of resistances to heat and mass transfer can be represented in a resistance network as shown in Figure 7.

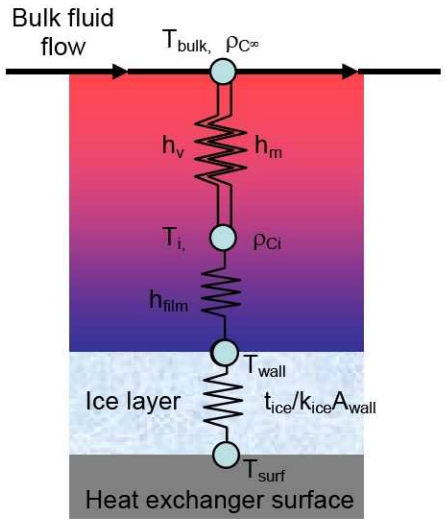


**Figure 7. Series/ parallel energy conduction description from a flow with condensate to the heat exchanger surfaces.**

In this network, $T_i$ is unknown and must be iteratively solved by equating the sum of the heat flows from the heat and mass transfer equations with the condensation heat flow [17]:

$$h_{film} (T_i - T_{wall}) = \dot{m}'' \Delta h_{fg} + h_v (T_{bulk} - T_i) \tag{24}$$

When ice is present $h_{film}$ is driven to a large value and functionally replaced with the resistance through the deposited ice layer.

*2. Ice Formation and Properties*

The mass transfer descriptions discussed above only describe the rate at which mass is deposited on the heat exchanger surfaces, the particular form of the deposition on surfaces is a separate matter. The final resistance to heat transfer in the CIHX as shown in Figure 7 is the ice resistance. Literature revealed no nondimensional correlations for ice properties for internal flows. The bulk of literature speaks to formation of ice on flat plates in external flow. While an external flow description may not be applicable in determining mass transfer, it is thought that the parameters of the formed ice should be independent of the particulars of the transport mechanism and are more dependant on properties such as the temperature under which the formation occurred, the amount of time that the ice has persisted, and the resulting density of the ice. This view is consistent with literature, and a collection of sources for ice properties given by Mago and Sherif [7] are used in modeling.

Ice density is very difficult to characterize. It is known that deposited ice begins as very low density hair-like structures which densifies as crystals grow at all depths in the ice layer due to penetration of moist gas and sublimation and redeposition of existing ice. For the case of deposition on time scales shorter than that in which significant redeposition can occur, a frost density function derived as a sole function of temperature has been proposed by Hayashi [18]:

$$\rho_f = 650 \exp(0.227 T_{wall}) \tag{25}$$

Where $\rho_f$ is the frost (ice) density and $T_{wall}$ is the ice surface temperature in degrees Celsius. This equation is recommended for application in air under the following conditions: frost surface temperature between -25 and 0°C, (248 K and 273 K), airstream velocities between 2 and 6 m/s, and an airstream humidity ratio equal to 0.0075 $kg_w/kg_a$ (or absolute humidity of 0.75%). It is unknown whether the continuous temperature change in the deposition temperature and the time frame will have a large effect on the ice density for the CIHX. Note that this compares to an absolute humidity of 3.5% or less for the CIHX which may alter this dependence. Additional consideration of the application of this correlation may be necessary if this resistance is found to be a dominant resistance. Also note that for 273 K, this equation yields an ice density of 650 $kg/m^3$, as compared to the value for fully dense ice of 919 $kg/m^3$. This implies that under no condition is the ice applied or densified to a smooth, fully dense layer. While this correlation was developed for use in air at atmospheric pressure, it is expected to be applicable for Oxygen at reduced temperature.

For the frost thermal conductivity $k_f$, an empirical correlation proposed by Yonko and Sepsy [19] is applied. This correlation is given by the equation:

$$k_f = 0.0242 + \left(0.000723 \rho_f\right) + \left(0.00000118 \rho_f^2\right) \tag{26}$$

This correlation is valid for frost densities less than 573 $kg/m^3$ corresponding to 272.45 K in Eqn. 30. The resulting conductivity at this temperature from the equation is 0.82 W/m-K. This compares to reported values of 1.8 to 2.3 W/m-K for fully dense ice at ~273 K. This is expected since frost is not deposited as solid, void free ice at any temperature. Figure 8 demonstrates a methodology developed to correct the values of density and conductivity as temperatures reach the melting temperature and surface tension densifies the ice by drawing liquid into the frost layer. The known values for ice density and conductivity at 273 K and the equation values up to 272.45 K are applied in the model and values are linearly interpolated between. This is implemented in SINDA/FLUINT by entering the data in a tabular form where it is automatically interpolated for use in calculation.

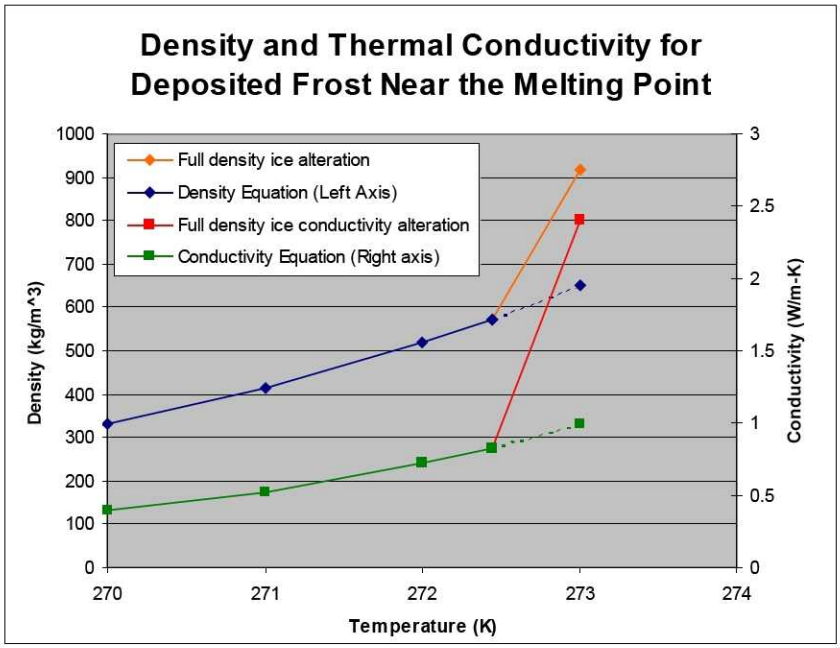


**Figure 8. Density and Thermal Conductivity based on given equations and altered properties based on fully dense ice at 273 K.**

With the density of the ice layer calculated, the resulting ice thickness is determined from:

$$\text{Ice thickness} = \left( \frac{m_{ice}}{\rho_f A_s} \right) \tag{27}$$

where $\rho_f$ is the ice density and $m_{ice}$ is the mass of ice stored in the domain, and As is the surface of that domain.

*3. Implementation in SINDA/FLUINT*

By default, all flows are homogeneous in SINDA/FLUINT. Thus all constituents, in any phase, travel at the same velocity as illustrated in Figure 9 (left). Condensate on a wall violates this assumption, since the condensate does not travel with the flow or does so much slower than the vapor flow. This situation requires that either the condensate mass be entirely removed from the flow, or by allowing slip flow between the gaseous and liquid phases. Slip flow is modeled in SINDA/FLUINT via the use of path twinning. Twinning of paths allows vapor and liquid phase paths to have differing velocities and is shown at the right in Figure 9. This is often used for describing annular flows. This mechanism is also applicable to the description of the case of the CIHX. When the wall temperature is above freezing and below the dew point, water will condense on the walls and, due to surface tension, will travel at a velocity much slower than the interior gaseous flow. If this movement is quick enough, it will simulate the removal of the water from the system via gravity. This functionality can also be simulated by species specific suction if the accumulated thickness is considered too great.

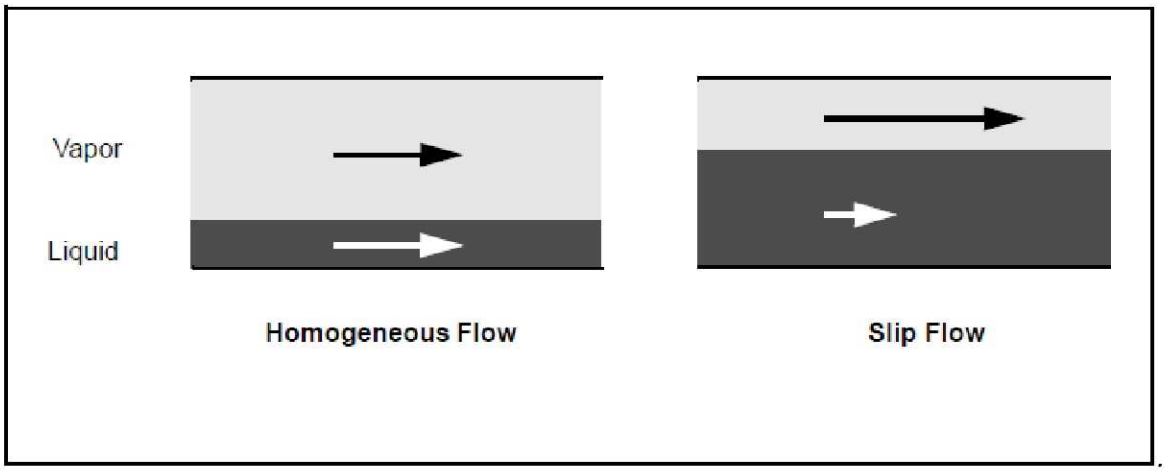


**Figure 9. Graphical description of slip flow allowed by a twinned path. [17]**

Modeling of the CIHX gets more complicated at and below the freezing temperature. In general, FLUINT does not handle solids. In the case of phase change to a solid, several approximations are used to make a liquid thermodynamically similar to a solid. First, the viscosity at and below freezing is dramatically increased, to the point that only very slow movement of the "solid fluid" on the wall occurs. To account for the freezing/sublimation energy, the specific heat is increased over a small temperature range. When integrated, this localized spike equals the freezing/sublimation energy. Below the freezing temperature, the specific heat is that of solid ice.

This given formulation accounts for heat and mass transfer from the fluid to the wall/ "solid fluid" interface, as well as energy storage and heat transport through the developed ice layer. However a significant hurdle remains in that C&R reports that the SINDA/FLUINT "solid fluid" approximation breaks down at temperature near 258 K due to the reliance of SINDA/FLUINT on NIST's REFPROP data where as the initial temperature of the CIHX is 235 K. At temperatures below 258 K, one of the properties calculated to develop the mass transfer results in a fatal error and the simulation terminates.

Fortunately, the equilibrium vapor pressure at 258 K is very low, thus the mass transfer rate from a warm saturated flow is largely unaffected by temperatures less than this value. A method is proposed involving temperature and property transformations to keep the simulated temperatures above 258 K during simulation while accounting for almost all of the mass transfer as well as most of the energy storage and heat transfer that would occur below this limit temperature. In this method, the properties of all model materials and fluids are transformed over a temperature range of interest.

In this case of the CIHX, in order to keep temperatures above 258 K, the temperatures in the range of 235 K to 265 K (a 30 K difference), are transformed (mapped) to a temperature between 260 and 265K, a 5 K difference. This ratio, 6 to 1 is then applied to the material properties of specific heat and conductivity in the transformed range. For specific heat, this ensures that the total integrated thermal mass is maintained at the transformed temperatures. Performing this transformation on the thermal conductivity likewise results in a larger heat transfer coefficient in Equation 23, offsetting the proportionally smaller difference in temperature. Since mass flow rate is directly proportional to the heat transfer rate as seen in Equation 24, this transformation is likewise carried over to mass transfer.

This transformation does give rise to two inaccuracies. First, while the material and gas properties are simple to transform due to their simple description in material and fluid databases, the water description is extremely complicated and transformation is not practical. Since the majority of the energy change between water as a vapor at 283 K and a solid at 265 K occurs in the phase changes, the effect on energy storage will vary minimally. The larger effect is in the amount of mass transferred. The mass transferred in Eq. 24 is a function of the difference in the free stream and saturation densities at the liquid (or solid) to vapor interface. Since these pressures can not be transformed (both due to complexity of this operation and for the reason that FLUINT can not handle lower

temperatures than 258 K) vapor pressures in the transformed range will be erroneously high. This error is highest at the minimum transformation temperature and is estimated to be a maximum of 15% for a surface at 235 K. Since the flow is a mixture of gas and water, the composite error is somewhat less due to the correct transformation of gas properties. The effect on the system energy balance is expected to be even lower since most of the water is expected to be removed within the CIHX, in this case somewhat further from the inlet.

## III. Conclusions

Sublimation, condensing/icing/melting, and flow through sorbent media (and the associated energy exchange) are all very complicated processes. Modeling any one of the processes that are experienced in the MTSA subassembly is a challenge in itself. Integrating their operation and capturing the coupling effects in a single thermal model is a further challenge. However, modeling to this level of detail is required if design optimization is to be realized, affording our space suit systems with light weight and efficient technology. Unfortunately, modeling tools such as SINDA/FLUINT and the Thermal Desktop interface do not have native routines for all of the physics that are needed to properly simulate the operation of the MTSA subassembly.

To address this, the methods presented lay the framework for describing the heat and mass exchange processes that occur in the three primary components of the MTSA subassembly. The described equations and logic can now be used to develop Thermal Desktop verification models which contain simplified geometry, boundary conditions, and flow inputs. These interim models verify operation of the code developed to simulate the physics of the three separate processes.

Each of the modeling methods contain assumptions that will require inputs or verification from testing. For example, the quasi-equilibrium adsorption assumption over predicts the rate at which the sorbent bed can adsorb $CO_2$ and limit rates for desorption are to date unknown. The density and thermal conductivity correlations assumed for deposited CIHX ice may result in more or less thermal resistance that will occur under MTSA conditions. In the SHX, the evaporation coefficient is poorly characterized yet key in the rate of heat removal from the system. In each of these cases the modeling methodologies allow for input of conservative values for the purposes of design and later refinement of those inputs as test data allows. Development of the interim models is expected to give insight into the design of possible intermediate tests aimed at refining model inputs and suggest testing procedures and instrumentation that can support model calibration.

The next step in the modeling process will be to build an integrated MTSA subassembly model. The verified code from the interim models will be applied to the relevant heat exchange surfaces and sorbent volumes in a fully discretized thermal model of the MTSA subassembly with geometry that represents the next design iteration. To simulate the operation of the full, two bed MTSA system, the completed subassembly model will be given inputs from a previously developed transient MTSA system model [10]. These simulations (the transient system model and the discretized model) allow evaluation of geometric and other design parameters in order to influence design of a prototype to be tested in a relevant environment later this year. Test data from this prototype will be used to verify and validate the developed subassembly and system models.

Several studies have been conducted to evaluate the feasibility of MTSA technology as well as simulate performance to influence the first design concepts. Implementation of the developed modeling methodologies is the next step in generating higher fidelity models that will allow a more realistic evaluation and design of a prototype–quality piece of hardware.

## References


[1]Iacomini, C. S., MacCallum, T., Morin, T, Straub-Lopez, K., Paul, H. L., "Martian Liquid CO2 and Metabolic Heat Regenerated Temperature Swing Adsorption for Portable Life Support Systems," *Space Technology and Applications International Forum (STAIF) 2007*, Albuquerque, N.M., Feb 11–15, 2007.

[2]Iacomini, C. S., Powers, A., Bower, C., Straub-Lopez, K., Anderson, G., MacCallum, T., Paul, H. L., "Model Calibration Experiments in Support of Metabolic Heat Regenerated Temperature Swing Adsorption Technology," *37th International Conference on Environmental Systems*, Chicago, IL, 2007-01-3273, 2007.

[3]Iacomini, C. S., Powers, A., Dunham, J., Straub-Lopez, K., Anderson, G., MacCallum, T., Paul, H. L., "Demonstration of Metabolic Heat Regenerated Temperature Swing Adsorption Technology," *37th International Conference on Environmental Systems*, Chicago, IL, 2007-01-3274, 2007.

[4]Iacomini, C. S., Powers, A., Lewis, M., Waguespack, G., Conger, B., Paul, H. L., "Testing, Modeling and System Impact of Metabolic Heat Regenerated Temperature Swing Adsorption," *38th International Conference on Environmental Systems*, San Francisco, CA, 2008-01-2116, 2008.

[5]Iacomini, C. S., Powers, A., and Paul, H. L., "PLSS Scale Demonstration of MTSA Temperature Swing Adsorption Bed Concept for CO2 Removal/Rejection", 2009-01-2388, 39th International Conference on Environmental Systems, Savannah, GA, July 12 -July 16, 2009.

[6]Padilla, S., Powers, A., Ball, T., Iacomini, C. S., and Paul, H. L., "Investigation of Condensing Ice Heat Exchangers for MTSA Technology Development", 2009-01-2387, 39th International Conference on Environmental Systems, Savannah, GA, July 12 -July 16, 2009.

[7]Mago, P. J., Sherif, S.A,. "Frost formation and heat transfer on a cold surface in ice fog," *International Journal of Refrigeration*, 28, (2005), 538-546.

[8] Reference data for the wash coating data of aluminum.

[9]ERG Aerospace, "Duocel Aluminum Foam," [online brochure] http://www.ergaerospace.com/foamproperties/literature/erg_duocel.pdf [Cited January 2010]

[10]Iacomini, C. S., Powers, A., Speight, G., Padilla, S., and Pual, H. L., " Transient Modeling and Analysis of a Metabolic Heat-Regenerated Temperature Swing Adsorption (MTSA) System for a PLSS," , *40th International Conference on Environmental Systems*, Barcelona, Spain, 2010-XX-XXXX, 2010.

[11]Hwang, G.-J., Yeh, R.-H., and Chao, C.-H., "Measurement of interstitial convective heat transfer and frictional drag for flow across metal foams," *Trans. ASME*, February 2002, 124, 120-129.

[12]Hardy, B., "Its-90 Formulations For Vapor Pressure, Frostpoint Temperature, Dewpoint Temperature, And Enhancement Factors In The Range –100 To +100 C," The Proceedings of the Third International Symposium on Humidity & Moisture, April 1998.

[13]Novikov, P. A., "Rate OF Sublimation Of Ice At Low Pressures," Translasted from *Inzhenerno-Fizicheskii Zhurnal*, Vol. 17, No. 5, pp. 861-865, November 1969.

[14]Fox, R. W., McDonald, A., *Introduction to Fluid Mechanics*, John Wiley & Sons, Inc., Ney York, 1998, Chap. 12.

[15]Korea Thermophysical Properties Data Bank, "Temperature Dependent Properties: Low P Gas Viscosity of WATER", *Chemical Engineering Research Information Center* [online database], URL: http://www.cheric.org/research/kdb/hcprop/showcoef.php?cmpid=1914&prop=VSG [Cited January 2010].

[16]Powers, A., "8029006NCTest Article Design Memo Final," June 26, 2008.

[17]Cullimore, B. A., Ring, S. G., Johnson, D. A., "SINDA/FLUINT User's Manual," C&R Technologies, Littleton, Colorado, Version 5.2, July 2009.

[18]Hayashi, Y. K. Aoki, H. Y., "Study of Frost Formation Based on a Theoretical Model of The Frost Layer," *Heat Transfer—Jpn* Res 6, No. 3, July–September, 1977, pp. 79–94.

[19]Yonko, J.D., Sepsy, C.F., "An Investigation of The Thermal Conductivity of Frost While Forming on a Flat Horizontal Plate," *ASHRAE Trans* 73, Part 2, June, Paper No. 2043, 1967, I.1.1.–I.1.11.